

Statistics and systematics of electron EDM searches with BaF

The NL-eEDM collaboration: A. Boeschoten^{1,2}, V.R. Marshall^{1,2}, T.B. Meijknecht^{1,2}, A.P. Touwen^{1,2}, P. Aggarwal^{1,2}, N. Balasubramanian^{1,2}, R. Bause^{1,2}, H. L. Bethlehem^{1,3}, A. Borschevsky^{1,2}, T.H. Fikkens^{1,2}, P.A.B. Haase^{1,2}, Y. Hao¹, S. Hoekstra^{1,2}, J.W.F. van Hofslot^{1,2}, S.A. Jones^{1,2}, K. Jungmann¹, J.E.J. Levenga^{1,2}, M.C. Mooij^{2,3}, H. Mulder^{1,2}, B.A. Nijman^{1,2}, E.H. Prinsen^{1,2}, B.J. Schellenberg^{1,2}, I.E. Thompson^{1,2}, R.G.E. Timmermans^{1,2}, L. van Sloten^{1,2}, W. Ubachs³, J. de Vries^{2,4}, L. Willmann^{1,2}, Y. Yin^{1,2}

¹ Van Swinderen Institute for Particle Physics and Gravity (VSI), University of Groningen, Nijenborgh 3, 9747 AG Groningen, The Netherlands

² Nikhef, National Institute for Subatomic Physics, Science Park 105, 1098 XG Amsterdam, The Netherlands

³ Department of Physics and Astronomy, LaserLaB, Vrije Universiteit, De Boelelaan 1100, 1081 HZ Amsterdam, The Netherlands

⁴ Institute for Theoretical Physics, University of Amsterdam, Science Park 904, 1098 XH Amsterdam, The Netherlands

January 30, 2026 / Received: date / Revised version: date

Abstract The NL-eEDM experiment searches for a non-zero electric dipole moment of the electron d_e (eEDM) in the ground state of barium monofluoride (BaF). A beam of BaF from a supersonic expansion source is probed with the spin precession method presented in [1]. This method permits the extraction of an eEDM value as well as values for parameters causing a possible systematic bias leading to a false eEDM. The currently achievable sensitivity is limited by statistics collected in a period of 34 hours and yields an d_e of $2(3) \times 10^{-25}$ e cm. Furthermore, from the same dataset sufficiently strong limits on parameters which can induce a false eEDM are extracted. These are mainly the electric field \mathbf{E} and the intensity of the lasers fields in the fiducial volume of the experiment. We summarize the steps required to upgrade of the experiment to reach a competitive level on d_e , e.g. an intense laser-cooled beam from a cryogenic buffer gas source and the light collection efficiency of fluorescence.

PACS. XX.XX.XX No PACS code given

1 Introduction

Searches for permanent electric dipole moments (EDMs) with composite systems, such as atoms and molecules, benefit from their high sensitivity to new interactions between elementary particles that violate both time-reversal (T) and parity (P) symmetry. Since for local quantum field theories T violation is equivalent to the violation of CP – the combination of charge conjugation (C) and parity – a nonzero EDM implies P,T and equivalently CP violation [2, 3, 4].

The Standard Model (SM) of particle physics (without neutrino masses) contains two terms that violate CP. It has long been experimentally established that CP is not conserved in flavor-changing weak interactions. In the SM this is parametrized by the complex phase in the Cabibbo-Kobayashi-Maskawa (CKM) quark-mixing matrix. The EDMs that result from this CKM phase are far too small to be detected at present [5, 6, 7]. However, the SM also contains the possibility of another, as yet unobserved source of T (CP) violation, which is the term parametrized by the “QCD vacuum angle” $\bar{\theta}$ [8]. The value of $\bar{\theta}$ is constrained to be less than about 10^{-10} by

the experimental upper limits on EDMs of the neutron [9] and the ^{199}Hg atom [10]. It is a persistent puzzle why the $\bar{\theta}$ parameter is so small.

New sources of CP violation are expected in scenarios that embed the SM in a more complete theory of particle physics. Such theories generically predict EDM values that are measurable in the ongoing or upcoming EDM experiments. In addition, in order to generate a matter-antimatter asymmetry observed in the universe, CP violation beyond the SM is required [11] assuming CPT to be a good symmetry [12]. For example, in electroweak baryogenesis [13], this typically leads to EDMs larger than SM predictions. The experimental discovery of EDMs would therefore be a major contribution to the road map towards improved models for particle physics.

The strongest constraints on the electron EDM (eEDM) in the last decade were obtained in paramagnetic diatomic molecules. Experiments with ThO molecules by the ACME collaboration [14] and with HfF⁺ molecular ions by the Boulder group [15] have provided new tight limits on the eEDM. Our experimental setup is partly similar to the experiment on YbF at Imperial College, London [16]. Our approach employs barium monofluoride (BaF) and dif-

Table 1: Searches for the e EDM in a number of different systems. Listed are the typical coherence times T and the resulting sensitivity in terms of the precession phase $\delta\phi$ [20].

System	$\delta\phi$ [rad]	T [s]	EDM limit [e cm] (95% c.l.)
Beam			
Tl [21]	1×10^{-6}	2.4×10^{-3}	$ d_{\text{Tl}} < 1.1 \times 10^{-24}$
ThO [14]	3×10^{-6}	1.0×10^{-3}	$ d_e < 1.31 \times 10^{-29}$
YbF [16]	4×10^{-5}	0.7×10^{-3}	$ d_e < 1.27 \times 10^{-27}$
BaF	1×10^{-3}	0.8×10^{-3}	$ d_e < 7 \times 10^{-25}$
Trap			
Ra [22]	3×10^{-3}	0.035	$ d_{\text{Ra}} < 5 \times 10^{-22}$
Yb [23]	1×10^{-3}	300	$ d_{\text{Yb}} < 1.5 \times 10^{-26}$
HfF ⁺ [15]	1×10^{-3}	3	$ d_e < 5 \times 10^{-30}$

fers in particular in methods addressing systematic biases in e EDM experiments. Experiments with paramagnetic molecules have the potential to improve their sensitivity to the e EDM in the coming years by several orders of magnitude. It has been shown recently that paramagnetic molecules provide not only the best limits on the e EDM and new CP-violating quark-electron interactions, but they can also be competitive with the neutron and diamagnetic atoms EDM searches in constraining hadronic sources of CP violation [17, 18].

This article reports on the implementation of the proposal for the NL- e EDM experiment [19] to search for the e EDM with BaF molecules. We present results of initial measurements performed with a beam from a supersonic source of BaF molecules as a proof-of-principle of the spin-precession method [1]. The method allows for the extraction of a number of systematic biases as well as a robust limit on a possible e EDM. We present the current sensitivity, which is limited by statistics, and we discuss ongoing upgrades to reach competitive levels with laser-cooled BaF molecules. We first discuss the setup of the NL- e EDM experiment, after which we present the results of the new spin-precession analysis method which was introduced in Ref. [1]. We conclude with a discussion of the prospects for the next phase of the experiment.

2 The NL- e EDM experiment

The NL- e EDM experiment utilizes a molecular beam of BaF and a novel spin-precession method, which provides access to key experimental parameters [1]. In paramagnetic diatomic molecular EDM experiments the measurements are sensitive to the induced molecular EDM $D^{P,T}$ [24, 25] which can be written as an enhanced electron EDM, i.e. $d_e P(E_{\text{ext}}) W_d \hbar / E_{\text{ext}}$, with the molecular CP-violation parameter W_d , the molecular polarization $P(E_{\text{ext}})$ in the external electric field E_{ext} . The molecular parameter W_d can be determined by molecular structure calculation. The size of the enhancement depends strongly on the molecular system and was recently calculated for BaF

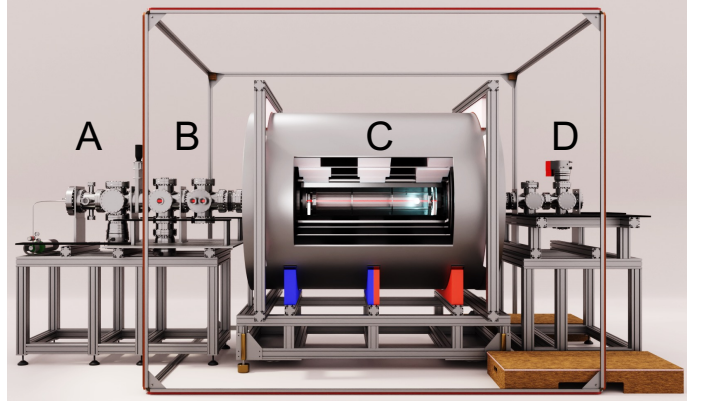


Figure 1: Overview of the modular experimental setup to scale. (A) Supersonic expansion source creating BaF molecules with a velocity of about 600m/s and a narrow velocity spread. The source is operated at repetition rates from 5–30 Hz. (B) Optical probing region for determination of the number of molecules and preparation of the molecules in a specific hyperfine state of the $X^2\Sigma^+$ ground state. These molecules enter (C) the region in which the spin-precession measurement is performed, consisting of a five layer magnetically shielded volume with magnetic fields of order $n\text{T}$ and electric fields of several kV/cm . The environmental fields of order $50\ \mu\text{T}$ are reduced to less than $5\ \mu\text{T}$ with rectangular field coils around the region. (D) The spin precession is read out by probing the population distribution in the two hyperfine states of the ground state.

[26]. In some atoms, this enhancement can reach values of 10^3 – 10^4 , while in molecules it can reach up to 10^9 [27].

The statistical sensitivity δd_e for the BaF e EDM experiment in a molecular beam is determined by the interplay of five quantities: The rate of detected molecules $\dot{n} = dn/dt$, the spin-precession time T , the measurement time T_{tot} , the degree of polarization of the molecule in an external electric field $P(E_{\text{ext}})$ and the value of the molecular parameter W_d for BaF, which has been determined to $W_d = 3.13 \pm 0.12 \times 10^{24}\text{Hz}/e\text{ cm}$ [26]. The sensitivity is given by

$$\delta d_e = \frac{1}{W_d P(E_{\text{ext}}) T \sqrt{\dot{n} P T_{\text{tot}}}}. \quad (1)$$

This uncertainty is derived from a phase determination in a spin-precession measurement $\delta\phi \approx 1/\sqrt{n_P}$ with n_P the total number of phase estimations [21]. In any experimental realization, this must be matched by an accurate determination of the parameters governing the measurement process [1].

We now discuss the spin-precession method with the connection to statistical sensitivity as well as possible systematic bias on an extraction of an e EDM limit. Then we show the experimental realization, which enables the exploitation of the method (Fig. 1) and the extraction of quantitative results (Sec. 3).

2.1 Spin-precession method

The measurement is performed in the $X^2\Sigma, v = 0, N = 0$ ground state of $^{138}\text{Ba}^{19}\text{F}$. The relevant states are hyperfine states $|F, m_F\rangle$ with the angular momentum $F = 0, 1$ and magnetic quantum number m_F . A superposition of these states is created by a two-photon process (Fig. 2) and can be written as

$$|\psi\rangle = \alpha |1, -1\rangle + \alpha' |1, 1\rangle + \beta |1, 0\rangle + \gamma |0, 0\rangle. \quad (2)$$

The coefficients α, α', β and γ are determined by the parameters of the two-photon process which are experimentally controlled. The parameters are the two-photon detuning from the hyperfine structure $\delta = (\omega_P - \omega_S) - \omega_{\text{HFS}}(E)$ in the range of kHz and detuning Δ from an excited state of order GHz. Furthermore, the length of the two-photon pulse t and the intensities of both laser fields determine the Rabi-frequencies $\Omega_{P/S}$ together with the polarizations of the laser fields $\hat{e}_{P/S}$. These parameters, together with the electric and magnetic fields \mathbf{E} and \mathbf{B} determine the evolution of the state $|\psi\rangle$. A second pulse after a time T is applied to project the superposition back to populations in $F = 0$ or $F = 1$. The probability $P_{0,1}$ of finding the molecule in $F = 0$ or $F = 1$ state is a function of the parameters,

$$P_{0,1} = P_{0,1}(\delta, \Delta, t, T, \Omega_{P/S}, \hat{e}_{P/S}, \mathbf{E}, \mathbf{B}), \quad (3)$$

which is numerically determined by solving the set of Optical Bloch equations [28] for the relevant eight states in external electric and magnetic fields (Fig. 2). The description provides the access to extract experimental parameters from the observed spin-precession signal and reduces the number of additional measurements for the determination of, e.g., the electric field strength, the spin-precession contrast or the Rabi frequencies $\Omega_{P/S}$ as we show Section 3.

In electric and magnetic fields the magnetic hyperfine states $|F, m_F\rangle = |1, \pm 1\rangle$ acquire a relative phase difference

$$\phi = (2\mu B/\hbar \pm d_e P(E_{\text{ext}}) W_d) T, \quad (4)$$

where the sign in front of the eEDM contribution depends on the relative orientation between the electric and magnetic field vector. The limit on the EDM of the BaF molecule is extracted from pairs of spin-precession measurements where the relative directions of the two fields have been reversed. Since the phase difference is extracted from measurements of the signal $P_{0,1}$ (Eq. 3), the dependence of $P_{0,1}$ on the experimental parameters has to be taken into account. We show that the experimental procedure permits the measurement of these parameters with sufficient precision to constrain a systematic bias on the eEDM determination.

2.2 Experimental implementation

2.2.1 Molecular beam source

Barium monofluoride (BaF) molecules are produced in a supersonic source. The source uses a rotating 3 mm wide

Ba disk with 40 mm diameter. Ba atoms are ablated by a pulsed Nd:YAG laser and seed a carrier gas of 2% SF₆ and 98% argon from a pulsed Even-Lavie valve. The source has a variable repetition rate typically set to 10 Hz and produces a molecular beam with a rotational temperature of 3.5 K. The mean velocity of the molecules is 600 m/s, with a velocity spread of about 35 m/s [29]. The average intensity is 3.3×10^9 molecules/sr/pulse, which is a factor ~ 5 higher compared to the intensity reported in [29]. The molecular beam pulse passes through a skimmer (diameter 5 mm) 28 cm after the exit of the Even-Lavie valve. Differential pumping provides for a vacuum pressure below 10^{-7} mbar downstream.

2.2.2 Control of magnetic and electric fields

A multilayer magnetic shielding has been constructed in order to provide a stable near-zero-field volume for performing the spin-precession measurement. The mu-metal shielding is designed with numerical simulation methods (COMSOL) in order to suppress external fields by 6 orders of magnitude. The fiducial volume has a 0.5 m diameter and 1.2 m length [30]. Additional suppression of external fields is achieved by large coils surrounding the shield, which compensate environmental fields in the laboratory of about 50 μT by a factor of 10. The magnetic field strength outside of the magnetic shield is constantly monitored with a resolution of better than $10 \text{ nT}/\sqrt{\text{Hz}}$. Variations of the external magnetic field are less than 100 nT over the course of the day. The suppression of external magnetic fields has been determined by exposing the shield to a bias field of $\pm 50 \mu\text{T}$ externally while measuring the magnetic field field change inside of the shielding with the spin-precession signal from the BaF molecules (Fig. 4). This suppression of six orders of magnitude leads to a magnetic field change of less than 100 fT in the course of a day.

The design of structures for generation of homogeneous \mathbf{E} and \mathbf{B} fields has been assisted by simulation (COMSOL) [30]. The magnetic holding field orthogonal with respect to the molecular beam of order 10 nT is generated by a cylindrical structure of 0.3 m diameter and length 1 m. A current distribution of $I(\theta) = I_0 \cos(\theta)$, with θ the azimuthal angle around the cylinder is generated by adjusting the wire density along the cylinder. This is known as a cosine-coil. The electric field parallel to the magnetic fields is generated by glass plates with a conductive coating (ITO) of 750 mm length and 100 mm height. The field plates are separated by 40 mm in a rigid construction of machinable ceramics (Macor) and glass.

The high voltage is provided by a positive and a negative high voltage supply (ISEG HPp/n 300 106). The electric field direction is reversed by a set of reed relays controlled via TTL signals from the experiments data and control system (DAQ) system. This permits a variable sequence of electric field direction and zero field while the power supplies are kept at constant voltage throughout the measurements in order to avoid time-dependent electric fields due to the limited voltage ramping rates. The field

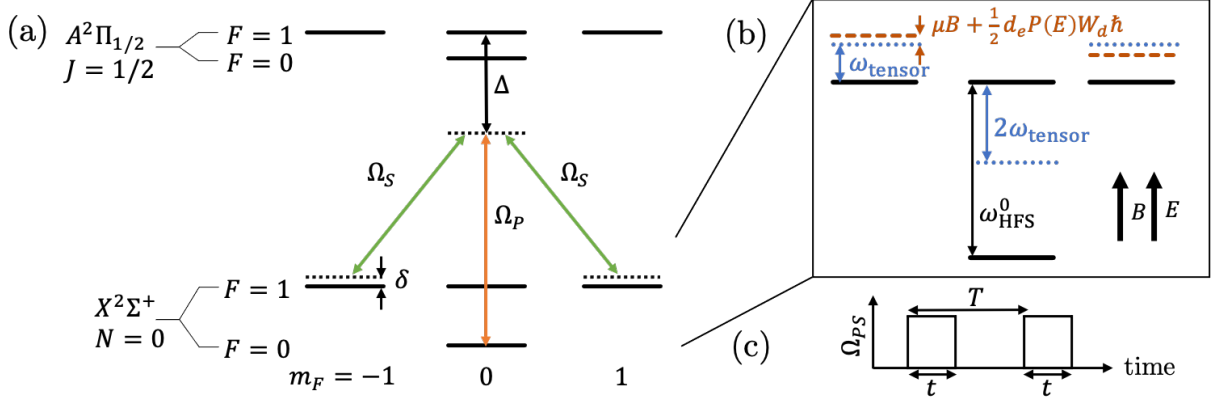


Figure 2: The superposition in the $X^2\Sigma^+$, $v = 0, N = 0, F = 1$ state is created by a two-photon transition via the electronically excited state $A^2\Pi_{1/2}, v = 0, J = 1/2$. The coupling is achieved by two laser fields with Rabi frequencies Ω_S and Ω_P at a typical detuning $\Delta = 1$ GHz from the $X^2\Sigma^+ - A^2\Pi_{1/2}$ resonance. The detuning $\delta = \omega_{PS} - \omega_{HFS}(E)$ is several kHz from two-photon resonance, where $\omega_{HFS}(E) = \omega_{HFS}^0 + \omega_{\text{tensor}}(E)$ and $\omega_{PS} = \omega_P - \omega_S$. (b) The $X^2\Sigma^+$, $v = 0, N = 0$ sublevels of the ground state in electric and magnetic fields. The hyperfine splitting in absence of external fields ω_{HFS}^0 is around 65.85 MHz. The tensor Stark shift of the $m_F = \pm 1$ levels, $\omega_{\text{tensor}}(E)$, is around 15 kHz at an electric field of 2 kV/cm. The tensor Stark shift of the $m_F = 0$ level is approximately twice that of ω_{tensor} with opposite sign. (c) The timing sequence of the laser-light pulses with effective Rabi frequency Ω_{PS} , where typical pulse lengths are $t = 80 \mu\text{s}$ and the pulse separation period is $T = 1 \text{ ms}$. Energy levels and timings are not to scale.

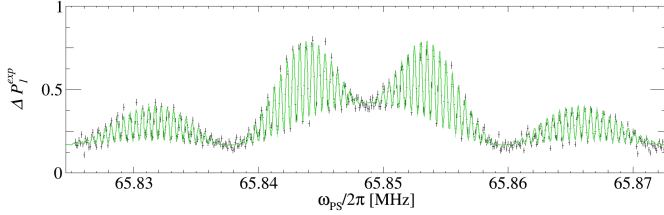


Figure 3: An example of the spin-precession signal $P_0(\delta)$ while keeping the parameters constant ($B = 4.40 \text{ nT}$, $E = 0 \text{ kV/cm}$, $t = 80 \mu\text{s}$ and $T = 2 \text{ ms}$). The green line is according to the model of Eq. 3. The hyperfine structure splitting in the ground state is $\omega_{HFS}^0 = 65.84854(3) \text{ MHz}$. The central fringes of the spectrum are most sensitive to a possible eEDM.

strength of several kV/cm is measured to an accuracy of order 1 V/cm with the spin-precession signal $P_0(\delta)$. This provides an absolute measurement of the field strength in the fiducial volume [1].

2.2.3 Laser frequency and stability

The light beams at multiple optical frequencies required in the experiment are provided by diode lasers and Ti:Sapph systems. The frequencies are controlled by a HighFinesse WS8-2 wavelength meter [31] in combination with a High-Finesse 8 channel photonic crystal switch to control up to 8 wavelengths simultaneously. A frequency stability sufficient for an experiment of better than 0.5 MHz over long periods ($> 10\text{h}$) is achieved [32]. The laser sources provide continuous wave output. Acousto-optical modulators

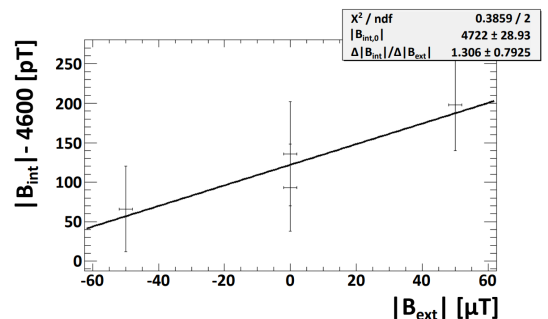


Figure 4: The magnetic field inside of the shielding is derived from spin-precession signals when the magnetic shield was exposed to a magnetic field change of $\pm 50 \mu\text{T}$. The field change inside the shielding was suppressed by $1.3(8) \times 10^{-6}$ in agreement with numerical simulations in COMSOL.

(AOMs) are employed to create pulses with controlled frequency offset and sub-ns timing. The RF-frequencies and the timing are derived from direct digital synthesis function generators, which are referenced to a GPS stabilized Rb-clock (SR FS725). Laser light at 815 nm is used for the determination of the molecular beam intensity on the $X^2\Sigma^+(v = 0, N = 1) - A^2\Pi_{3/2}(v = 0, J = 3/2)$ transition by laser induced fluorescence in Section B (Fig. 1) and counts per molecular pulse n_{norm} is recorded by the DAQ. Rotational pumping from the $X^2\Sigma^+(v = 0)$ $N = 2$ state to $N = 0$ state and hyperfine optical pumping of the $X^2\Sigma^+(N = 0)$ $F = 1$ to $F = 0$ state employs light at 860 nm also in Section B. The population in the $X^2\Sigma^+(v = 0, N = 0, F = 1)$ state after the spin

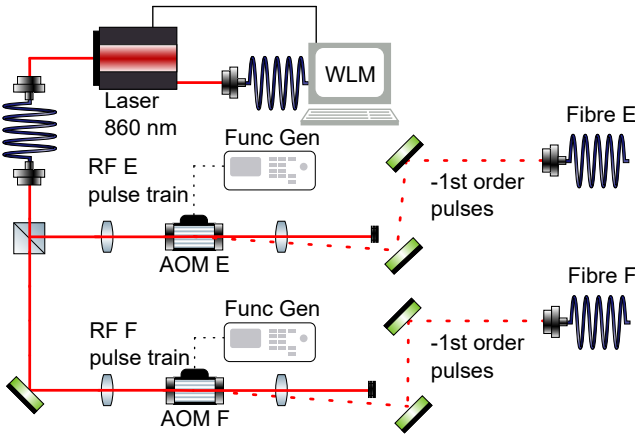


Figure 5: Pulses with precise timing and phase coherence for the spin-precession methods are generated from light of one laser at 860 nm (TOPTICA TApro). The light is split by a beam splitter into two beams. Each beam is passed through an AOM which is driven by RF pulses generated DDS function generators referenced to a GPS controlled Rb-clock. The pulsed 1st order beams of each AOM are aligned into optical fibers E and F.

precession is probed with the $X^2\Sigma^+, N = 0, F = 1 - A^2\Pi_{3/2}, J = 3/2, F = 1$ transition in Section D (Fig. 1). The counts n_{sp} is also recorded to allow for the experimental determination of P_1 (Eq. 3).

The number of detected photons is $n_{\text{sp}} = \epsilon n_{\text{molecules}}$, where the detection efficiency $\epsilon = 7 \times 10^{-4}$ results from the solid angle of light collection and the quantum efficiency of the detector. The counts are recorded within timing bins of $100 \mu\text{s}$, which corresponds to 10 m/s resolution on the velocity of the molecules. Integrated over the velocity profile of the beam, we observe about 100 photons per molecular pulse. However, the average yield during the data taking was 20 photons/pulse due to the degradation of the molecular yield from the source over the course of several hours.

The laser pulses for the superposition creation and readout (see Fig. 2) are derived from a single laser at a wavelength of 860nm with a pair of acousto optical modulators (AOMs) (Fig. 5). These light fields for the coupling to the spin-precession state are delivered by beams counter-propagating to the molecular beam, providing for light pulse intensity (Rabi frequency Ω_{PS}) and timing (t and T) independent of the molecular velocity. Parameters such as laser frequency, intensity, pulse lengths and timing are recorded by the data acquisition system with the spin-precession data for every single molecular pulse.

2.2.4 From fluorescence detection to spin-precession signal

The signal counts per molecular pulse n_{norm} provides a measurement of the number of produced molecules, while the counts n_{sp} detected during the time of flight window between 6 and 7 ms yields the number of molecules in

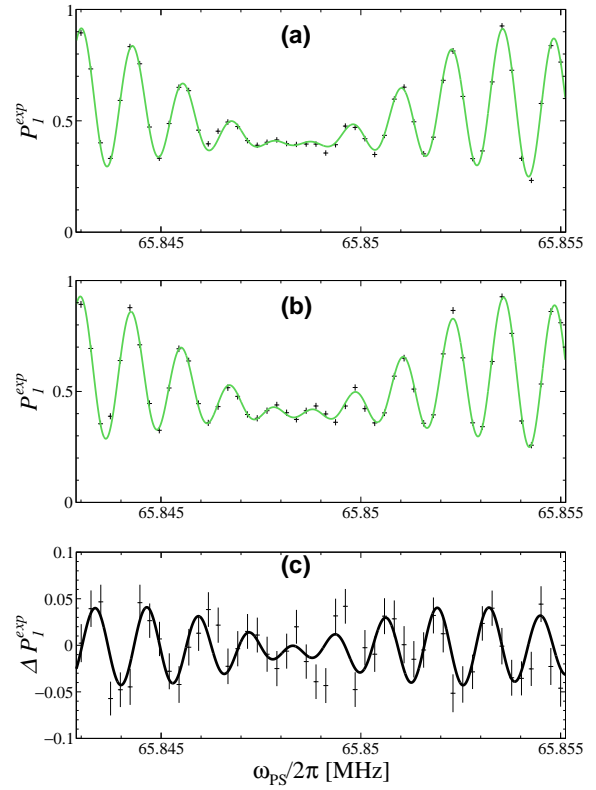


Figure 6: Spin-precession signals for (a) molecules with velocity $600 \pm 6 \text{ m/s}$ and (b) $576 \pm 6 \text{ m/s}$. The Rabi frequency Ω_{PS} differs due to the Doppler shift contribution to the detuning Δ . (c) The change of Δ of 24 MHz causes a $3.0(5)\%$ change in Ω_{PS} which results in a dependence of ΔP_1^{exp} on the frequency ω_{PS} .

the hyperfine state $F = 1$ after spin precession. The spin-precession P_1 (Eq. 3) is determined in the experiment by

$$P_1^{\text{exp}} = n_{\text{sp}} / (f \cdot n_{\text{norm}}), \quad (5)$$

with a calibration factor f which is determined when we do not drive the spin precession. The sum of the populations in the hyperfine states $|1, -1\rangle$ and $|1, 1\rangle$ is determined with a statistical uncertainty which is given by counting statistics. The uncertainty of a measurement, e.g. Fig. 8, is determined by counting statistics including the background from scattered light.

3 Spin-precession analysis

Data collected within 2 days is evaluated for extracting the current sensitivity of the experimental setup. Parameters during the measurement were set at the start and data collection continued automated (Table 2). During the data taking, the values for the detuning δ span over 12 kHz in 50 steps in order to record spin-precession signals $P_1(\delta)$ such as in Figs. 6, 7 and 8. The electric field direction was reversed every 150 s, which corresponds to 50 steps

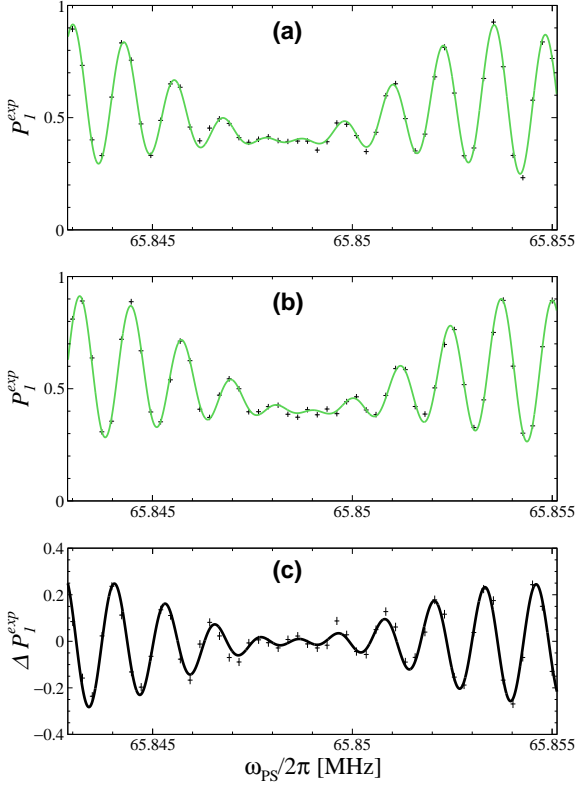


Figure 7: Spin-precession signals for (a) electric field parallel and (b) antiparallel to the magnetic field. The electric field strength was different by about 1 %. (c) The difference in field strength causes a dependence of ΔP_1^{exp} on the frequency ω_{PS} . A change of field strength of $-23.0(2)$ V/cm at a field of 1.970 kV/cm is extracted.

Parameter	# Values	Parameter Range
Timing	1	$t = 80 \mu\text{s}$, $T = 1 \text{ ms}$
δ	50	$\pm 6 \text{ kHz}$
E	2	$-1.947(1)$ and $+1.970(1)$ kV/cm
B	2	$-4.715(12)$ nT, $+5.462(12)$ nT
Ω_{PS}	5	$\pm 3\%$
n_{sp}	10 – 100	per ablation pulse

Table 2: List of the different experimental conditions during the collection of data in about 34 h.

in δ . The magnetic field reversal was done only after 24 h in order to reduce effects from hysteresis in the magnetic shielding. The field reversal resulted in a different field strength. Parameters related to the timing of the pulse sequence are set to an accuracy better than 1 ns by function generators to a low phase noise which are referenced to a GPS disciplined Rb-clock. Frequencies of all the lasers are controlled by a wavelength meter to a precision of better than 1 MHz. Parameters of the measurement (Table 3) are either controlled to the required accuracy or are extracted from the observed spin-precession fitted against the model function P_1 (Eq. 3).

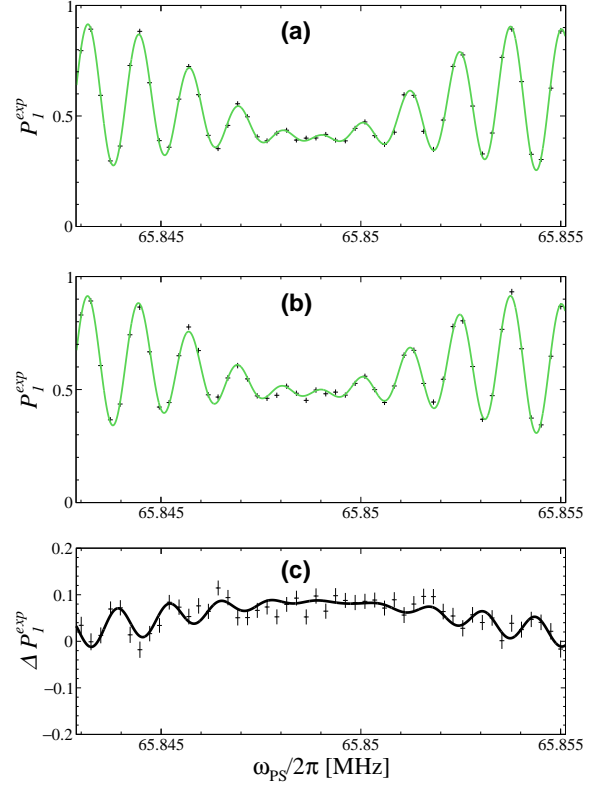


Figure 8: Spin-precession signals for (a) a magnetic holding field of $-4.71(1)$ nT and (b) $5.46(1)$ nT. The two spectra were recorded 23 h apart. (c) The difference of the signal ΔP_1^{exp} yields a difference in magnetic field strength of $0.72(3)$ nT and a change of $1.0(4)\%$ in Ω_{PS} for these two datasets.

The *e*EDM contribution is derived from the difference of measurements with parallel and anti-parallel electric and magnetic fields. The magnetic field strength is chosen to provide for a phase around $\phi = \pi/2$ (Eq. 4) and a phase error of $\delta\phi \approx \delta P_1^{\text{exp}}$ can be extracted. A measurement at a single detuning $\delta \approx 0$ kHz would require independent experimental determination of other parameters such as **E**, Ω_{PS} and the contrast of the signal for a reliable extraction of an *e*EDM limit. The advantage of the method presented here is that the signal Eq. 3 provides sensitivity to all these parameters. We generate a set of spectra from one dataset (Figs. 6, 7 and 8), from molecular pulses which have specific combinations of the parameters such as **E**, **B** and Ω_{PS} at the time of analysis. The spectra are analyzed with the spin-precession model $P_1(\delta)$ with a typical reduced χ^2 in the range of $0.9 – 1.3$. The precision of the parameters, including the contrast are limited by the same statistics and are sufficient to constrain a systematic bias on the *e*EDM (Table 3). The results presented in this paper are based on an effective measurement time of 17 h for each direction of the magnetic field. The electron *e*EDM $d_e = 2(3) \times 10^{-25} e \text{ cm}$ has been extracted from the dataset and the sensitivity is in agreement with the collected statistics.

Parameter	Constraint	$\delta d_e < 10^{-27} e \text{ cm}$	Source
t	$< 1 \text{ ns}$	5 ns	clock
T	$< 1 \text{ ns}$	100 ns	clock
δ	$< 1 \text{ Hz}$	16 Hz	clock
Δ	$< 1 \text{ MHz}$	5 MHz	WLM
\mathbf{E}	$dE/E < 2 \times 10^{-3}$	$< 2 \times 10^{-3}$	stat.
\mathbf{B}	$\delta B < 10 \text{ pT}$	$< 0.1 \text{ pT}$	stat.
Ω_{PS}	$d\Omega/\Omega < 5 \times 10^{-3}$	$< 2 \times 10^{-3}$	stat.

Table 3: Summary of parameters controlled the experimental implementation (pulse length t , spin-precession time T and frequency δ) together with measured parameters, such as laser frequencies controlled by wavelength meter (WLM) and statistical limits of electric and magnetic field and the Rabi frequency. The accuracy of the latter depend on the same statistics as the limit on the eEDM. The third column gives the requirements to constrain a systematic bias on a limit on d_e . The last column give the method by which the constraint can be achieved.

4 Prospects for the next phase

Various improvements to the experimental configuration can be implemented – or are already in the process of being implemented – to increase the statistical sensitivity of an eEDM-search represented by Eq. (1). In particular, by using slower molecules we increase the spin-precession T . In phase 2 of our experiment we replace the supersonic beam source with a laser-cooled, hexapole-focused, cryogenic buffer gas beam [33].

In a cryogenic buffer gas beam (CBGB) source [34], molecular radicals are produced inside a cold cell via laser ablation of a solid target. The molecules are cooled through collisions with continuously flowing helium or neon buffer gas. Entrained in this gas, they are extracted from the cell to form a cold molecular beam. Based on the design in [35], we have constructed a cryogenic buffer gas source that generates pulses containing typically 2×10^{10} BaF molecules in the state $N = 0$, with a brightness of 1×10^{11} molecules per sr per pulse at a velocity of 200 m/s [36]. To create an intense, collimated beam, we will use a combination of an electrostatic hexapole lens, which provides a position-dependent force, and transverse laser cooling, which provides a velocity-dependent friction force. Electrostatic multipole lenses have been widely used for state selection and focusing of light polar molecules [37]. We have recently demonstrated [38] that a properly designed hexapole lens significantly enhances the intensity of the downstream BaF beam.

BaF, like its lighter homologous CaF and SrF, possesses a structure amenable to laser cooling. Calculations predict that the ground vibrational level of $A^2\Pi_{1/2}$ decays to the ground vibrational level of $X^2\Sigma^+$ with a branching ratio of 0.964 [39]. We recently reported the first demonstration of transverse Doppler cooling of a hexapole-focused BaF beam [33]. Using three tunable lasers with appropriate sidebands and detuning, the molecules scattered approximately 400 photons, limited by scattering rate and the available interaction time. The leakage of the pop-

ulation to dark states was less than 10%. The observed scattering rate was 14% of the theoretical maximum, but this can likely be improved by optimizing sideband power and refining the magnetic field in the cooling region. The experimental results also served to benchmark trajectory simulations, which we use to predict the achievable flux for the eEDM experiment. Our simulations indicate that incorporating the hexapole lens together with the laser cooling stage could increase the molecular flux by two orders of magnitude with respect to the supersonic beam source. The detection of the signal n_{sp} will be upgraded from the $X^2\Sigma^+ - A^2\Pi_{3/2}$ transition to the $X^2\Sigma^+ - D^2\Sigma^+$ transition at a wavelength of 405 nm. The excited state $D^2\Sigma^+$ primarily decays via the $A^2\Pi$ states by emission of two infrared photons. In addition, the detection will change from a photomultiplier to an avalanche photodiode based detection with an increased solid angle for the light collection.

A comparison between the current ‘phase 1’ experiment and the next stage ‘phase 2’ experiment is given in Table 4. The considerable increase in the projected average photon rate (s^{-1}) is the consequence of significant combined improvements in the source intensity, the implementation of transverse laser cooling, and an improved fluorescence detection scheme. Because of the increased length of the molecular pulse from the cryogenic source the fraction of molecules taking part in the spin precession will be reduced by a factor 3. Combined, these factors leads to the indicated average photon counting rate. The square root of the photons counts in a day, multiplied with the increased polarization factor in a higher electric field strength, the increased precession time, the interference contrast and the W_d parameter of the BaF molecule (see Equation 1) leads to the associated statistical sensitivities ($e \text{ cm day}^{-1}$) that are given at the bottom of the table.

5 Conclusion

The spin-precession technique developed in the NL-eEDM [1] demonstrated a statistically limited determination of an eEDM $d_e = 2(3) \times 10^{-25} e \text{ cm}$ in the first phase. Additionally, the method allows for a determination of experimental parameters such as Rabi frequency Ω_{PS} and electric field strengths from the same dataset. Their uncertainty permits limiting of the systematic bias to well below the eEDM limit. Improved statistics in future measurement will further limit the eEDM and the uncertainties in the experimental parameters.

It is attractive to use a longer spin precession time T , as the sensitivity improves linearly with this parameter. Until recently, increasing the interaction time was accompanied by a significant decrease in the counting rate \dot{N} . However, recent advances in decelerating molecular beams [40, 41, 42, 43] combined with spectacular progress in molecular laser cooling [44] and the demonstration of intense cryogenic molecular beam sources [45] have opened a route to circumvent this limitation and make long interaction times possible. Ultimately, we aim perform our experiment on barium-containing molecules in a fountain [46]

Table 4: Summary of achieved performance of the parts of the experiment (phase 1) and the projected gain in statistical sensitivity for phase 2.

Item	Phase 1	Phase 2	Comment
Molecular Beam Source			
Source type	supersonic [29]	cryogenic buffer gas [36]	
Brightness (molecules/sr/pulse)	3.3×10^9	1×10^{11}	in $N = 0$
Repetition rate (Hz)	10	20	
Forward velocity (m/s)	600 ± 30	200 ± 30	velocity (m/s $\pm 1\sigma$ spread)
Laser Cooling			
Transverse cooling	1	200	gain hexapole and laser cooling
Rotational cooling	1	10	gain optical pumping
Spin Precession Parameters			
Electric Field (kV/cm)	2	10	
Polarization factor $P(E_{\text{ext}})$	0.16	0.53	resulting from larger field strength
Precession Time (ms)	1	3	Due to reduced velocity
Precession fraction	0.9	0.3	Due to length of molecular pulse
Interference contrast	0.9	0.9	
Fluorescence Detection			
Signal n_{sp}	1	1.5	Change detection via $\Pi_{3/2}$ to $D^2\Sigma^+$ state
Light collection	0.02	0.20	Solid angle of light collection
Quantum efficiency	0.07	0.80	Change from PMT to APD
Average photon rate (s $^{-1}$)	200	2×10^9	
Statistical sensitivity (e cm day $^{-1}$)	5×10^{-25}	2×10^{-29}	

or in an optical lattice trap [47]. A similar approach has recently been suggested for the YbF molecule [48].

6 Acknowledgments

This work is financed by the Netherlands Organisation for Scientific Research (NWO) as part of the research programme ‘Physics beyond the Standard Model with cold molecules’ with project number 166, project VI.C.212.016 and project OCENW.XL21.XL21.074.

7 Author contributions

All authors have contributed through discussions and corrections to the final manuscript.

References

1. A. Boeschoten, V. R. Marshall, T. B. Meijknecht, A. Touwen, H. L. Bethlem, A. Borschevsky, S. Hoekstra, J. W. F. van Hofslot, K. Jungmann, M. C. Mooij, R. G. E. Timmermans, W. Ubachs, and L. Willmann. Spin-precession method for sensitive electric dipole moment searches. *Phys. Rev. A*, 110:L010801, Jul 2024.
2. M. Pospelov and A. Ritz. Electric dipole moments as probes of new physics. *Annals of Physics*, 318(1):119 – 169, 2005.
3. K. Jungmann. Searching for electric dipole moments. *Ann. d. Physik*, 525(8-9):550–564, 2013.
4. J. Engel, M. J. Ramsey-Musolf, and U. van Kolck. Electric dipole moments of nucleons, nuclei, and atoms: The standard model and beyond. *Progress in Particle and Nuclear Physics*, 71(Supplement C):21 – 74, 2013.
5. I. B. Khriplovich and A. R. Zhitnitsky. What Is the Value of the Neutron Electric Dipole Moment in the Kobayashi-Maskawa Model? *Phys. Lett. B*, 109:490–492, 1982.
6. F. Hoogeveen. The Standard Model Prediction for the Electric Dipole Moment of the Electron. *Nucl. Phys. B*, 341:322–340, 1990.
7. Y. Ema, T. Gao, and M. Pospelov. Standard Model Prediction for Paramagnetic Electric Dipole Moments. *Phys. Rev. Lett.*, 129(23):231801, 2022.
8. G. 't Hooft. Computation of the Quantum Effects Due to a Four-Dimensional Pseudoparticle. *Phys. Rev. D*, 14:3432–3450, 1976. [Erratum: Phys.Rev.D 18, 2199 (1978)].
9. C. Abel, S. Afach, N. J. Ayres, C. A. Baker, G. Ban, G. Bison, K. Bodek, V. Bondar, M. Burghoff, E. Chanel, Z. Chowdhuri, P.-J. Chiu, B. Clement, C. B. Crawford, M. Daum, S. Emmenegger, L. Ferraris-Bouchez, M. Fertl, P. Flaux, B. Franke, A. Fratangelo, P. Geltenbort, K. Green, W. C. Griffith, M. van der Grinten, Z. D. Grujić, P. G. Harris, L. Hayen, W. Heil, R. Henneck, V. Hélaine, N. Hild, Z. Hodge, M. Horras, P. Iaydjiev, S. N. Ivanov, M. Kasprzak, Y. Kermaidic, K. Kirch, A. Knecht, P. Knowles, H.-C. Koch, P. A. Koss,

S. Komposch, A. Kozela, A. Kraft, J. Krempel, M. Kuźniak, B. Lauss, T. Lefort, Y. Lemière, A. Leredde, P. Mohamurthy, A. Mtchedlishvili, M. Musgrave, O. Naviliat-Cuncic, D. Pais, F. M. Piegsa, E. Pierre, G. Pignol, C. Plonka-Spehr, P. N. Prashanth, G. Quéméner, M. Rawlik, D. Rebreyend, I. Rienäcker, D. Ries, S. Roccia, G. Rogel, D. Rozpedzik, A. Schnabel, P. Schmidt-Wellenburg, N. Severijns, D. Shiers, R. Tavakoli Dinani, J. A. Thorne, R. Virot, J. Voigt, A. Weis, E. Wursten, G. Wyszynski, J. Zejma, J. Zenner, and G. Zsigmond. Measurement of the permanent electric dipole moment of the neutron. *Phys. Rev. Lett.*, 124:081803, Feb 2020.

10. B. Graner, Y. Chen, E. G. Lindahl, and B. R. Heckel. Reduced limit on the permanent electric dipole moment of ^{199}Hg . *Phys. Rev. Lett.*, 116:161601, Apr 2016.

11. A. D. Sakharov. Violation of CP invariance, C asymmetry, and baryon asymmetry of the universe. *Pisma Zh. Eksp. Teor. Fiz.*, 5:32–35, 1967.

12. O. Bertolami, Don Colladay, V. Alan Kostelecky, and R. Potting. CPT violation and baryogenesis. *Phys. Lett. B*, 395:178–183, 1997.

13. J. van de Vis, J. de Vries, and M. Postma. Bubble Trouble: a Review on Electroweak Baryogenesis. *ArXiv*, page 2506.19069, 2025.

14. V. Andreev, D. G. Ang, D. DeMille, J. M. Doyle, G. Gabrielse, J. Haefner, N. R. Hutzler, Z. Lasner, C. Meisenhelder, B. R. O’Leary, C. D. Panda, A. D. West, E. P. West, and X. Wu. Improved limit on the electric dipole moment of the electron. *Nature*, 562(7727):355–360, 2018.

15. T. S. Roussy, L. Caldwell, T. Wright, W. B. Cairncross, Y. Shagam, K. B. Ng, N. Schlossberger, S. Y. Park, A. Wang, J. Ye, and E. A. Cornell. An improved bound on the electron’s electric dipole moment. *Science*, 381(6653):46–50, 2023.

16. J. J. Hudson, D. M. Kara, I. J. Smallman, B. E. Sauer, M. R. Tarbutt, and E. A. Hinds. Improved measurement of the shape of the electron. *Nature*, 473:493–496, 2011.

17. V. V. Flambaum, M. Pospelov, A. Ritz, and Y. V. Stadnik. Sensitivity of EDM experiments in paramagnetic atoms and molecules to hadronic CP violation. *Phys. Rev. D*, 102(3):035001, 2020.

18. H. Mulder, R. G. E. Timmermans, and J. de Vries. Probing the QCD $\bar{\theta}$ term with paramagnetic molecules. *JHEP*, 07:232, 2025.

19. P. Aggarwal, H. L. Bethlem, A. Borschevsky, M. Dennis, K. Esajas, P. A. B. Haase, Y. Hao, S. Hoekstra, K. Jungmann, Th. B. Meijknecht, M. C. Mooij, R. G. E. Timmermans, W. Ubachs, L. Willmann, and A. Zapara. Measuring the electric dipole moment of the electron in BaF. *The European Physical Journal D*, 72(11):197, Nov 2018.

20. A. Boeschoten and L. Willmann. Perspectives on electric dipole moments of atoms and molecules. In *EPJ Web of Conferences*, volume 282, page 01019. EDP Sciences, 2023.

21. B. C. Regan, E. D. Commins, C. J. Schmidt, and D. DeMille. New limit on the electron electric dipole moment. *Phys. Rev. Lett.*, 88:071805, 2002.

22. R. H. Parker, M. R. Dietrich, M. R. Kalita, N. D. Lemke, K. G. Bailey, M. Bishof, J. P. Greene, R. J. Holt, W. Korsch, Z.-T. Lu, P. Mueller, T. P. O’Connor, and J. T. Singh. First measurement of the atomic electric dipole moment of ^{225}Ra . *Phys. Rev. Lett.*, 114:233002, 2015.

23. T. A. Zheng, Y. A. Yang, S.-Z. Wang, J. T. Singh, Z.-X. Xiong, T. Xia, and Z.-T. Lu. Measurement of the electric dipole moment of ^{171}Yb atoms in an optical dipole trap. *Phys. Rev. Lett.*, 129:083001, 2022.

24. P. G. H. Sandars. The electric dipole moment of an atom. *Phys. Lett.*, 14(3):194 – 196, 1965.

25. P. G. H. Sandars. Measurability of the proton electric dipole moment. *Phys. Rev. Lett.*, 19:1396–1398, 1967.

26. P.A.B. Haase, D.J. Doeglas, A. Boeschoten, E. Eliav, M. Ilias, P. Aggarwal, H. L. Bethlem, A. Borschevsky, K. Esajas, Y. Hao, S. Hoekstra, V.R. Marshall, Th. Meijknecht, M. Mooij, K. Steinebach, R.G.E. Timmermans, A. Touwen, W. Ubachs, L. Willmann, and Y. Yin. Systematic study and uncertainty evaluation of P,T-odd relativistic enhancement factors in BaF. *J. Chem. Phys.*, 155:034309, 2021.

27. V. A. Dzuba and V. V. Flambaum. Parity violation and electric dipole moments in atoms and molecules. *Int. J. Mod. Phys. E*, 21(11):1230010, 2012.

28. Alexander Boeschoten. *Precision measurements in diatomic molecules: a route to a permanent electric dipole moment*. PhD thesis, University of Groningen, 2023.

29. P. Aggarwal, H. L. Bethlem, A. Boeschoten, A. Borschevsky, K. Esajas, Y. Hao, S. Hoekstra, K. Jungmann, V. R. Marshall, T. B. Meijknecht, M. C. Mooij, R. G. E. Timmermans, A. Touwen, W. Ubachs, L. Willmann, Y. Yin, and A. Zapara. A supersonic laser ablation beam source with narrow velocity spreads. *Review of Scientific Instruments*, 92(03):033202, 2021.

30. Thomas Meijknecht. *Electric and Magnetic Field Control for Electric Dipole Moment Searches*. PhD thesis, University of Groningen, 2023.

31. *Technical Information Wavelength Meter WS8-2*, Mar 2021.

32. Virginia Rose Marshall. *Spectroscopy and Systematic Effects: an eEDM experiment using BaF molecules*. PhD thesis, University of Groningen, 2024.

33. J. W. F. van Hofslot, I. E. Thompson, A. Touwen, N. Balasubramanian, R. Bause, H. L. Bethlem, A. Borschevsky, T. H. Fikkens, S. Hoekstra, S. A. Jones, J. E. J. Levenga, M. C. Mooij, H. Mulder, B. A. Nijman, E. H. Prinsen, B. J. Schellenberg, L. van Sloten, R. G. E. Timmermans, W. Ubachs, J. de Vries, and L. Willmann. 2D transverse laser cooling of a hexapole focused beam of cold BaF molecules. *ArXiv*, page 2506.19069, 2025.

34. N. R. Hutzler, H.-I. Lu, and J. M. Doyle. The buffer gas beam: An intense, cold, and slow source for atoms and molecules. *Chem. Rev.*, 112(9):4803–4827, 2012.
35. S. Truppe, M. Hambach, S. M. Skoff, N. E. Bulleid, J. S. Bumby, R. J. Hendricks, E. A. Hinds, B. E. Sauer, and M. R. Tarbutt. A buffer gas beam source for short, intense and slow molecular pulses. *J. Mod. Optics*, 65(5-6):648–656, 2018.
36. M. C. Mooij, H. L. Bethlem, A. Boeschoten, A. Borschevsky, K. Esajas, T. H. Fikkens, S. Hoekstra, J. W. F. van Hofslot, K. Jungmann, V. R. Marshall, T. B. Meijknecht, R. G. E. Timmermans, A. Touwen, W. Ubachs, L. Willmann, Y. Yin, and NL eEDM collaboration. Influence of source parameters on the longitudinal phase-space distribution of a pulsed cryogenic beam of barium fluoride molecules. *New Journal of Physics*, 26(5):053009, 2024.
37. S. Y. T. van de Meerakker, H. L. Bethlem, N. Vanhaecke, and G. Meijer. Manipulation and control of molecular beams. *Chem. Rev.*, 112(9):4828–4878, 2012.
38. A. Touwen, J. W. F. van Hofslot, T. Qualm, R. Borchers, R. Bause, H. L. Bethlem, A. Boeschoten, A. Borschevsky, T. H. Fikkens, S. Hoekstra, K. Jungmann, V. R. Marshall, T. B. Meijknecht, M. C. Mooij, R. G. E. Timmermans, W. Ubachs, L. Willmann, and NL eEDM collaboration. Manipulating a beam of barium fluoride molecules using an electrostatic hexapole. *New Journal of Physics*, 26(7):073054, 2024.
39. Y. Hao, L. F. Paštka, L. Visscher, P. Aggarwal, H. L. Bethlem, A. Boeschoten, A. Borschevsky, M. Denis, K. Esajas, S. Hoekstra, K. Jungmann, V. R. Marshall, T. B. Meijknecht, M. C. Mooij, R. G. E. Timmermans, A. Touwen, W. Ubachs, L. Willmann, Y. Yin, A. Zappa, and (NL-eEDM Collaboration). High accuracy theoretical investigations of CaF, SrF, and BaF and implications for laser-cooling. *J. Chem. Phys.*, 151(3):034302, 2019.
40. A. Osterwalder, S.A. Meek, G. Hammer, H. Haak, and G. Meijer. Deceleration of neutral molecules in macroscopic traveling traps. *Phys. Rev. A*, 81(5):051401, May 2010.
41. N. E. Bulleid, R. J. Hendricks, E. A. Hinds, S. A. Meek, G. Meijer, A. Osterwalder, and M. R. Tarbutt. Traveling-wave deceleration of heavy polar molecules in low-field-seeking states. *Phys. Rev. A*, 86(2):021404, 2012.
42. M. Quintero-Pérez, T. E. Wall, S. Hoekstra, and H. L. Bethlem. Preparation of an ultra-cold sample of ammonia molecules for precision measurements. *J. Mol. Spectr.*, 300:112 – 115, 2014.
43. J. E. van den Berg, S. C. Mathavan, C. Meinema, J. Nauta, T. H. Nijbroek, K. Jungmann, H. L. Bethlem, and S. Hoekstra. Traveling-wave deceleration of SrF molecules. *J. Mol. Spectros.*, 300:22 – 25, 2014.
44. E. S. Shuman, J. F. Barry, and D. DeMille. Laser cooling of a diatomic molecule. *Nature*, 467:820–823, 2010.
45. D. Patterson and J. M. Doyle. Bright, guided molecular beam with hydrodynamic enhancement. *J. Chem. Phys.*, 126(15):154307, 2007.
46. C. Cheng, A. P. P. van der Poel, P. Jansen, M. Quintero-Pérez, T. E. Wall, W. Ubachs, and H. L. Bethlem. Molecular fountain. *Phys. Rev. Lett.*, 117:253201, 2016.
47. R. Bause, N. Balasubramanian, T. Fikkens, E. H. Prinsen, K. Steinebach, A. Jadbabaie, N. R. Hutzler, I. A. Aucar, L. F. Paštka, A. Borschevsky, and S. Hoekstra. Prospects for measuring the electron’s electric dipole moment with polyatomic molecules in an optical lattice. *Phys. Rev. A*, 111:062815, 2025.
48. J. Lim, J. R. Almond, M. A. Trigatzis, J. A. Devlin, N. J. Fitch, B. E. Sauer, M. R. Tarbutt, and E. A. Hinds. Laser cooled YbF molecules for measuring the electron’s electric dipole moment. *Phys. Rev. Lett.*, 120:123201, 2018.